Computational Materials Science 152 (2018) 256–261

Contents lists available at ScienceDirect

Computational Materials Science

journal homepage: www.elsevier.com/locate/commatsci

Lattice-matched heterojunctions between blue phosphorene and MXene Y_2CX_2 (X = F, O, and Y = Zr, Hf)

Geng Li[a,b], Yinchang Zhao[c], Shuming Zeng[a,b], M. Zulfiqar[a,b], Lin-Wang Wang[d], Jun Ni[a,b,*]

[a] State Key Laboratory of Low-Dimensional Quantum Physics, Department of Physics, Tsinghua University, Beijing 100084, People's Republic of China
[b] Collaborative Innovation Center of Quantum Matter, Beijing 100084, People's Republic of China
[c] Department of Physics, Yantai University, Yantai 264005, People's Republic of China
[d] Materials Sciences Division, Lawrence Berkeley National Laboratory, Berkeley, CA 94720, United States

ARTICLE INFO

Keywords:
Heterojunctions
Blue phosphorene
MXene
Electronic properties
Flat band

ABSTRACT

We use *ab initio* calculations to explore the geometry, bonding and electronic properties of Mxene/blue phosphorene (BLP) heterobilayers. Perfect lattice-matched and energetically stable Mxene/BLP heterobilayers are firstly predicted to be vertically stacked with less than 1% lattice mismatch. The electronic properties of the heterobilayers are consistent with the substrate Mxene and the states projected on the isolated components are preserved. The unchanged electronic properties for the components upon the formation of the heterobilayers indicate the physical vdW interaction between the BLP monolayers and Mxene sheet, instead of the chemical bonds. The most stable BLP/Y_2CX_2 (X = O, and Y = Hf, Zr) are found to be a semiconductor with a type-II band alignment where the excited electrons and holes are localized in different layers. However, for BLP/Y_2CX_2 (X = F, and Y = Hf, Zr), the most stable structure is metallic with a strong band bending which lead to the existence of a partial flat band along the Γ point to the M point that mainly originates from the BLP monolayes. The appearance of the spatial separation of electron and hole and the partial flat band in these heterostructures have potential applications in optoelectronic devices and strong electron-electron correlation field. Our analysis also suggests that Mxene is a promising substrate to grow BLP monolayer epitaxially.

1. Introduction

As the rapid development of the experimental techniques, graphene-like two-dimensional (2D) materials – silicene [1–3], hexagonal boron nitride (hBN) [4,5], transition-metal dichalcogenides (TMDCs) [6–8], MXenes [9,10], black and blue phosphorene [11,12], borophene [13,14], etc. – have been synthesized [15]. These single-layer 2D materials possess various significant electronic and optical properties which have potential applications for the next generation of nanoscale semiconductor devices, energy storage materials, solar battery materials, and chemical catalyst [16–20]. For instance, the family of 2D transition metal carbides, carbonitrides, and nitrides (collectively referred to as MXenes), which can be produced by the etching out of the layers from the MAX phases [9,10], have shown a promising performance in lithium (Li)-ion batteries and supercapacitors, exhibiting volumetric capacitances of over 300 farads per cubic centimetre that exceed those of most previously reported materials [9,17]. A previous first-principles study has shown that all of the bare MXenes are metallic. However, after functionalization, some of the MXenes, such as Ti_2CO_2, Zr_2CO_2, and Hf_2CO_2, become semiconductors with band gaps ranging from 0.24 eV to 1.80 eV, and some (Zr_2CF_2 and Hf_2CF_2) still preserves the metallic property [10].

After the successful synthesis of a single-layer black phosphorus arranged in a hexagonal puckered lattice [11], a new phase of a single-layer BLP with a buckle structure like silicene has also been realized by the molecular beam epitaxial growth on Au(1 1 1) surfaces using black phosphorus as precursor [12]. The electronic bandgap of the single layer blue phosphorus on Au(1 1 1) is determined to be 1.10 eV by scanning tunneling spectroscopy measurement [12]. The formation energy of BLP is only a few meV higher than that of black phosphorene and both types of phosphorenes can transform with each other in the process of fabrication [21].

Currently, van der Waals heterostructures stacked by the different families of 2D atomic sheets are considered as a novel way to construct the nanoelectronic and optoelectronic devices and form the interfaces where the novel states and exotic physical phenomena may emerge [15,22,23]. For example, a truly two-dimensional nanotransistor has been constructed using heterostructures of graphene, MoS_2, and hexagonal boron nitride, where graphene acts as both source or drain and gate electrodes, hCBN as the high-k dielectric, and MoS_2 as the channel

* Corresponding author at: State Key Laboratory of Low-Dimensional Quantum Physics, Department of Physics, Tsinghua University, Beijing 100084, People's Republic of China.
E-mail address: junni@mail.tsinghua.edu.cn (J. Ni).

https://doi.org/10.1016/j.commatsci.2018.05.040
Received 28 February 2018; Received in revised form 10 May 2018; Accepted 19 May 2018
Available online 22 June 2018
0927-0256/

[24,25]. In addition, the heterostructure graphene/hBN has been fabricated and observed the emergence of second-generation Dirac cones (SDCs), which has been used for the realization of Hofstadter butterfly states [26]. Although numerous 2D vdW heterostructures have been found, lattice-matched and energetically stable heterostructures are still attractive in experiment. The heterostructures formed with lattice-dismatched 2D materials lead to the electron inhomogeneous distribution and surface distortion, which decreases the carrier mobility.

In this study, we have investigated six inequivalent BLP/Mxene heterostructures using the density-functional theory (DFT) method. BLP/Mxene are formed to the lattice-matched semiconductor/semiconductor and semiconductor/metal 2D vdW heterojunctions. Both systems have a perfect lattice match and the lattice mismatch is less than 1%. Although the previous works [22,23] have systematically studied the electronic structures and interface properties of heterojunctions composed of BLP and Zr-, Hf-, and Nb-based Mxenes, there are some differences and new results in our work. The BLP/Y_2CX_2 (X = O, and Y = Hf, Zr) atop-II keep a semiconductor while the BLP/Y_2CX_2 (X = F, and Y = Hf, Zr) atop-II become metals. In high-precision calculations, we found that the conduction band and the valence band for the semiconducting heterobilayers are from the Mxene and BLP sheets, respectively. The type-II band heterojunctions form when they are stacked on each other, which is in contrast with the results of the previous works [22,23]. The emergence of the flat band under the semiconductor/metal contacts result from the strong band bending of the CBM from BLP monolayer.

The paper is organized as follows: Calculation details are described in Section 2. The structural and electronic properties of single-layer BLP and Mxene structures are presented in Section 3. In Section 3, we determine the different stacking patterns and calculate the electronic properties for the energetically favorable heterobilayers. Section 4 is the summary.

2. Methods

Our calculations are performed in the frame of the density-functional theory (DFT) [27] with the generalized gradient corrected Perdew-Burke-Ernzerhof (PBE) [28] exchange-correlation functional. The plane-wave basis projector augmented wave (PAW) method [29,30] is employed to describe the ion-electron interactions, implemented in the Vienna *ab initio*simulation package (VASP) [31,32]. Because of the absence of strong bonding, a damped van der Waals (vdW) correction (DFT-D2) [33] is adopted to consider the nonbonding forces. At the same time, the inherent underestimation of the band gap given by DFT is also corrected by using the Heyd-Scuseria-Ernzerhof (HSE) [34] screened-nonlocal-exchange functional of the generalized Kohn-Sham scheme. Analysis of the charge transfers between the heterojunctions is determined by the Bader technique [35]. The plane-wave cutoff is taken to be 520 eV and a vacuum spacing of more than 20 Å is taken to prevent interactions between adjacent images. The energy convergence threshold for electronic iteration is set to be 10^{-5} eV. All the geometries and lattice parameters are fully relaxed using the conjugate gradient algorithm until the Hellmann-Feynman forces on each atom are less than 10^{-2} eV/Å. The Brillouin zone (BZ) is sampled by a Monkhorst-Pack [36] k-point mesh of 18 × 18 × 1 for the structure relaxations, while a k-grid of 32 × 32 × 1 is generated for the static calculations and density of state (DOS) calculations, respectively. Phonon frequencies are calculated based on the density functional perturbation theory (DFPT) [37], implemented in the PHONOPY code [38] and interfaced to VASP with a supercell of 4 × 4 × 1.

3. Single-layer BLP and Mxene

Before analysis of bilayer heterostructures of BLP and Mxene, the structural and electronic properties of the monolayer constituents are studied. The top and side view of the 2 × 2 supercell for the hexagonal monolayer BLP and Mxene are shown in Fig. 1(a)-(c), respectively.

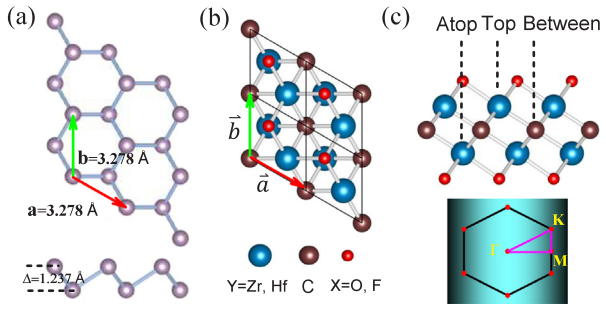

Fig. 1. (a) Top view (up) and side view (down) of 2 × 2 × 1 monolayer BLP. Top and lateral view of the Y_2CX_2 monolayer structures are shown in (b) and (c), respectively. The colors denote different elements, as seen in (b). The Brillouin zone (BZ) and high-symmetry paths corresponding to the unit cell are shown in (c).

First, BLP belongs to the space group C_{3v} with the lattice constant of 3.278 Å. Our calculated buckle height is 1.237 Å, which is consistent with the experiment value of 1.18 Å. The electronic structure calculated with the GGA and HSE06 functionals and phonon spectrum are shown in Fig. 2(a). The buckled monolayer BLP has an indirect band gap of 1.946 eV, while the HSE06 correction has a larger band gap of 2.525 eV, where the valance band maximum (VBM) and the conduction band minimum (CBM) lie along the Γ-M direction in BZ, respectively. The states at the vicinity of the Fermi level originate from the 3*p* orbitals of the P atoms. The work function for BLP is found to be 5.957 eV.

The structural, electronic properties and phonon spectrum of the AA configurations (see S1 in Ref. [39]) of Mxene Y_2CX_2 (X = F, O, and Y = Zr, Hf) used for the other building-block of heterobilayer are presented in Figs. 1(b), (c) and 2(b)-(e). The four structures belong to the $P\bar{3}m1$ space group and the lattice parameters vary from 3.306 Å to 3.266 Å, which perfectly match to the BLP. For F atoms decorated Mxene Y_2CX_2 (X = F, and Y = Zr, Hf), the systems calculated within GGA and HSE06 are metals. The states near the Fermi level are composed of the *d* orbitals of Y (Y = Zr, Hf). Similar to BLP, Mxene Y_2CX_2 (X = O, and Y = Zr, Hf) are found to be an indirect band-gap semiconductor with a band gap of 0.965 eV and 1.207 eV, respectively. The HSE06 correction band gaps are 1.083 eV and 1.123 eV for Zr_2CO_2 and Hf_2CO_2, respectively. The VBM and CBM of both systems reside at the Γ point and M point in BZ, respectively. The states in VBM are mostly contributed from 2*p* orbitals of C atoms and *d* orbitals of Y (Y = Zr, Hf) atoms. However, those in CBM are mostly from the *p* and *d* orbitals of Y atoms. The work functions for the four structures are 5.246 eV, 3.930 eV, 5.187 eV and 3.534 eV, respectively, as listed in Table 1. There is no imaginary frequency on the calculated phonon spectrums for BLP and Mxene, which indicates the structures are stable thermally.

4. Bilayer heterostructures

The calculated lattice constants and space groups of BLP and Mxene Y_2CX_2 (X = F, and Y = Zr, Hf) are very close to each other, which gives a good reason to use these monolayers as the building blocks to construct vdW heterostructures. We define the binding energy using the following formula: $E_{bind} = E_{BLP} + E_{Mxene} - E_{Hetro}$, where E_{BLP}, E_{Mxene}, and E_{Hetro} represent the total energy of BLP, Mxene and their heterostructures, respectively. By comparing the binding energies of six symmetry stacking patterns, we determine the energetically favorable structure for each configuration (see S2 in Ref. [39]). For the heterobilayers with the substrate Mxene decorated with O atoms, they favor to the atop-II pattern, while the ground states of heterobilayers with the constituent layers of Mxene Y_2CF_2(Y = Zr, Hf) are hcp-II pattern. The lattice mismatches for the four optimized ground state structures are found to be 1%, 0.85%, 0.4%, 0.4%, respectively.

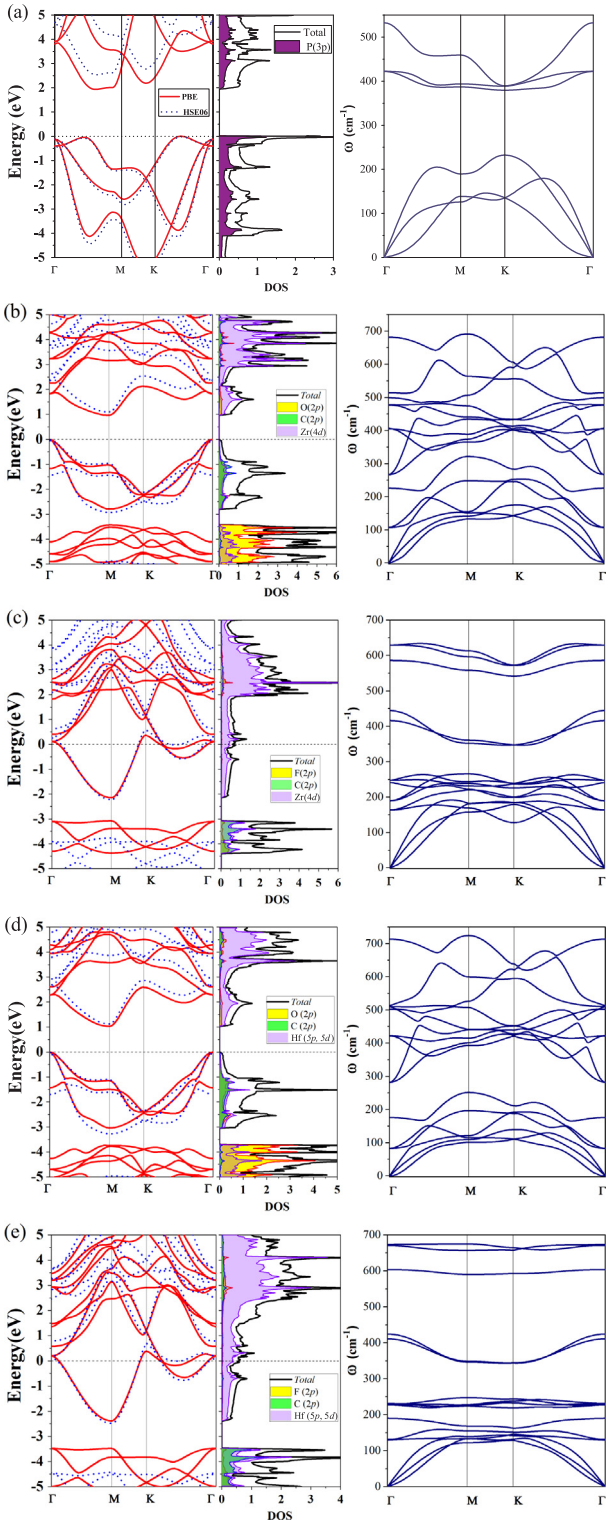

Fig. 2. Electronic structure (Band structure, DOS, and PDOS) and phonon dispersion for the optimized monolayer of (a) BLP, (b) Zr_2CO_2, (c) Zr_2CF_2, (d) Hf_2CO_2, (c) Hf_2CF_2. The band structure depicted with red-solid lines and blue-dashed curves are calculated within the GGA and HSE06 functionals, respectively. The black-dashed lines correspond to the Fermi level. (For interpretation of the references to color in this figure legend, the reader is referred to the web version of this article.)

After the determination of the optimized structure for each heterostructure configuration, the structural, energetic and electronic properties under inclusion of the vdW correction are calculated, as

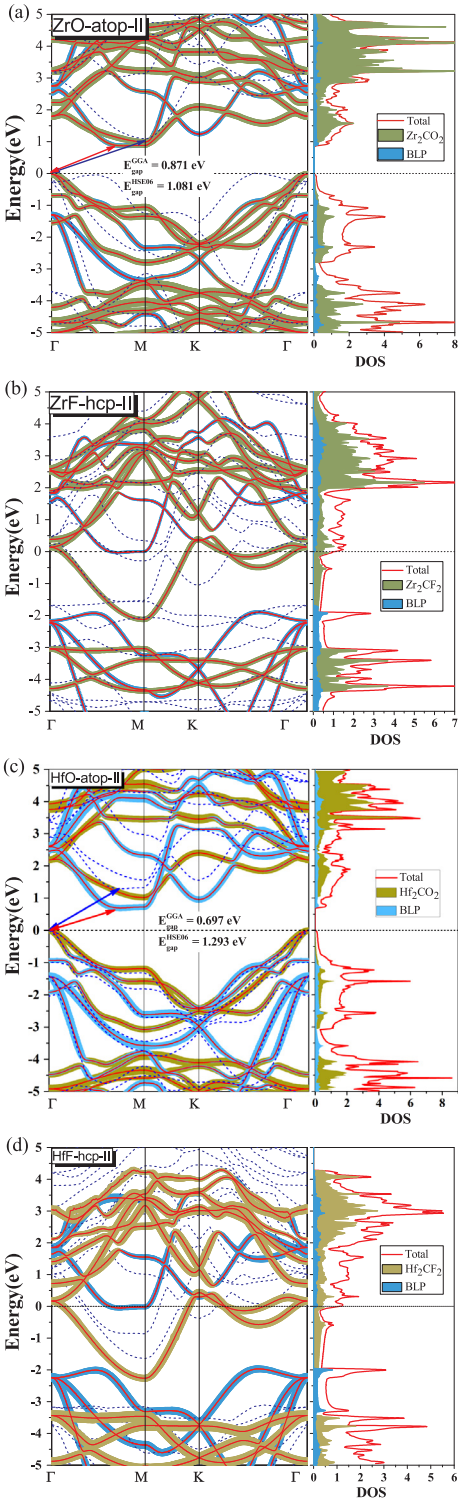

Fig. 3. The band structures (left) and the corresponding DOS (right) projected on BLP and Mxene calculated with GGA for (a) BLP/Zr_2CO_2 atop-II, (b) BLP/Zr_2CF_2 hcp-II, (c) BLP/Hf_2CO_2 atop-II and (d) BLP/Hf_2CF_2 hcp-II, respectively. The Fermi energy (E_F) level (black dashed line) is set to the valence band maximum.

displayed in Fig. 3(a)-(d) and demonstrated in Table 1. According to Table 1, the geometric structures (lattice constant, bond length and buckle height) of the constituent layers of the heterostructures change a little when compared with their isolated forms. The interlayer spacings, which are defined as the perpendicular distances from the surface X atoms on Mxene to the bottom P atom plane, are 2.752 Å, 2.691Å,

Table 1
Calculated ground-state properties for monolayer and their heterobilayer structures. The stable structures, lattice parameters of primitive unit cell a and b (see Fig. 1), the bond lengthes between X and Y d_{X-Y}, and Y and C d_{Y-C}, the layer distances for the heterobilayers d, buckle heights for BLP Δ, binding energies E_{bind} (per unit cell), total amounts of charge transfer from Y_2CX_2 to BLP $\Delta\rho$, band gaps of the structures calculated within GGA (E_g^{GGA}) and HSE06 (E_g^{HSE}), work functions Φ determined from Y_2CX_2 side, and lattice mismatches (LM).

	Geometry	$a = b$ (Å)	d_{X-Y} (Å)	d_{Y-C} (Å)	d (Å)	Δ (Å)	E_{bind} (eV)	$\Delta\rho$ (e)	E_g^{GGA} (eV)	E_g^{HSE} (eV)	Φ (eV)	LM
BLP	–	3.278	–	–	–	1.237	–	–	1.946	2.525	5.957	–
Zr_2CO_2	–	3.310	2.120	2.368	–	4.635	–	–	0.965	1.083	5.246	–
BLP/Zr_2CO_2	atop-II	3.309	2.113	2.366	2.725	1.225	1.635	0.020	0.871	1.081	4.975	1%
Zr_2CF_2	–	3.306	2.328	2.271	–	5.129	–	–	metal	metal	3.930	–
BLP/Zr_2CF_2	hcp-II	3.305	2.310	2.276	2.691	1.222	1.548	0.014	metal	metal	4.119	0.85%
Hf_2CO_2	–	3.266	2.101	2.335	–	4.606	–	–	1.027	1.123	5.187	–
BLP/Hf_2CO_2	atop-II	3.281	2.095	2.352	2.689	1.229	2.893	0.082	0.697	1.293	4.701	0.4%
Hf_2CF_2	–	3.266	2.313	2.235	–	5.079	–	–	metal	metal	3.534	–
BLP/Hf_2CF_2	hcp-II	3.287	2.283	2.243	2.526	1.217	2.740	0.003	metal	metal	3.881	0.4%

2.689 Å, 2.526 Å for BLP/Y_2CX_2 (X = O, F, and Y = Zr, Hf) hybrid systems, respectively. The vertical distances are larger than the sum of the covalent radii of the P and O/F atoms, which indicates that there are no chemical bonds at the interface region. The Bader charge analysis for the charge transfers $\Delta\rho$ (less than 0.1 e) from Mxene to BLP demonstrates that there is no depletion from one layer to the other for all the stacking geometries. This result is expected due to the weak vdW interaction between the individual layers. The binding energies for BLP/Y_2CX_2 (X = O, F, and Y = Zr, Hf) heterostructures are 1.64, 1.55, 2.89, and 2.74 eV per unit cell, respectively. Those values of binding energy are larger than these in the previous works [22,23] but have the same order of magnitude as other van der Waals (vdW) crystals [44–46], which also suggest the weak vdW interlayer interactions between Mxene and BLP.

In order to understand the details of the bonding mechanism in the two examined heterobiayers, we have calculated the charge density difference and the plane-averaged charge density difference $\Delta\rho(z)$ to visualize the electron redistribution upon the formation of the heterobilayers (see FIG.S2 and FIG.S3 in Ref. [39]), which directly proves the existence of the weak vdW interlayer interactions between Mxene and BLP. The calculated work function for the BLP monolaye is 5.957 eV, which is larger than the those for Mxene. Thus, the electrons inject from Mxene to BLP. The Bader charge analysis exhibit that there are about 0.020, 0.014, 0.082 and 0.003 electrons transferred from Mxene to BLP in the BLP/Zr_2CO_2 atop-II, BLP/Zr_2CO_2 hcp-II, BLP/Hf_2CO_2 atop-II and BLP/Zr_2CF_2 hcp-II, respectively. This surplus charge accumulation also results in the formation of a weak built-in electronic field between the interface [40]. The interface dipoles are also very common for vdW heterostructures [41,42].

Due to the weak vdW interaction between the heterobilayers, the electronic states of Mxene and BLP are weakly changed by the formation of the heterobilayers. All calculated systems keep the similar properties with the substrate Mxene and they are non-magnetic. The band structures and DOS projected on the BLP monolayer and Mxene sheet within the GGA and HSE06 correction are calculated, as shown in Fig. 3(a) and (b). The heterobilayers BLP/Y_2CX_2 (X = O, and Y = Zr, Hf) atop-II are semiconductors with an indirect band gap. Although the interaction between these two layers is weak, there is a significant decrease in the GGA band gap when these two single layers are stacked on top of each other. The band gap with GGA for BLP/Zr_2CO_2 atop-II and BLP/Hf_2CO_2 atop-II are 0.871 eV and 0.697 eV respectively. The HSE06 gaps for both heterobilayes (1.081 eV for BLP/Zr_2CO_2 atop-II, 1.293 eV for BLP/Hf_2CO_2 atop-II) are larger than GGA gaps. But they are close to the HSE06 gaps of the Mxene. According to the band structures projected on the isolated layers, we found that the VBM for both heterobilayes localized at the Γ point originate from the Y_2CX_2 (X = O, and Y = Zr, Hf) layer while the CBM lying between the Γ point and the M point in BZ mainly arise from the BLP sheet. The partial DOSs also indicate that the excited electrons and holes for the heterolayers can be confined in the Mxene and BLP sheet, respectively. The spatial separation of electrons-holes in the heterobilayers with the indirect band gap result in the formation of the long-lived excitons, which have a big potential application for optoelectronics devices and solar battery [43].

Due to the semiconducting feature of Y_2CX_2 (X = O, and Y = Zr, Hf) and BLP, the formation of atomically stacking structures are equivalent to the semiconductor/semiconductor contacts. Considering the band alignments for both interfaces, we align the energy levels of the two examined interfaces with the reference of the vacuum level V_∞ and get the detailed insight into the CBM and VBM shifts, as depicted in Fig. 4(e). The valence/conduction band offsets of the Y_2CX_2 (X = O, and Y = Zr, Hf) and BLP are 0.87/0.02 eV, 0.93/0.33 eV, respectively. The nature of the type-II is that the two band edges come from different individual layers and consequently, the excited electrons and holes are confined in different layers [44]. We can conclude that similar to Mg$(OH)_2$/WS_2 [44], InSe/phosphorene [45] and h-AlN/Mg$(OH)_2$ van derWaals bilayer heterostructures [46], the interfaces of our systems present a Type-II heterojunction. The previous works reported that BLP/Y_2CX_2 (X = O, and Y = Zr, Hf) herterostures are Type-I and both VBM and CBM come from the Mxene [22,23]. They showed that the VBM locates at the M point which is mainly contributed from the Mxene, while we showed the VBM lies between the Γ and M points mainly from BLP, which may be caused by the more dense k points and larger cutoff energy used in our calculations. Due to the band alignments, the work-functions for the heterobilayers are smaller than those of both constituent monolayers. The calculated work functions of the heterobilayers on the sides of Mxene are 4.975 eV and 4.701 eV for

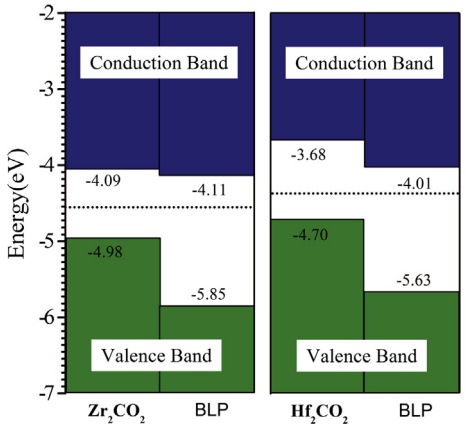

Fig. 4. The band alignments of the monolayers for Zr_2CO_2 atop-II (left) and Hf_2CO_2 atop-II (right) where the vacuum level of both monolayer materials are set to be 0 eV. The CBM and VBM of both compounds are highlighted in blue and green regions. (For interpretation of the references to color in this figure legend, the reader is referred to the web version of this article.)

BLP/Zr_2CO_2 atop-II and Hf_2CO_2 atop-II, respectively.

Similar to the electronic properties of the substrate Mxene, the heterobilayers BLP/Y_2CX_2 (X = F, and Y = Zr, Hf) hcp-II keep metallic type. In Fig. 3(c) and (d), we present the electronic structures of the hybrid interfaces, including the projection of the electronic states on the isolated monolayers. Due to the tiny Bader charge transfer and the weak interlayer vdW interaction, the energy bands contributed from the Mxene and BLP near the Fermi level are well preserved in the formation of the heterobilayers. However, a careful analysis shows that the weak interlayer interaction and the lattice stretch for the BLP monolayer result in a band gap decrease of 0.10 eV and 0.03 eV compared with the band-gap value of 1.946 eV of the pristine BLP in BLP/Zr_2CF_2 hcp-II and BLP/Hf_2CF_2 hcp-II, respectively. By the inspection of the band structures projected on the BLP and Mxene in Fig. 3(c) and (d), we find that the positions of VBM and CBM for the BLP in both heterobilayers decrease a lot when compared with the pristine BLP and there occurs a band bending at the interface region as both isolated sheets move together. The band bending can be estimated using the difference between the Fermi levels of the hybrid systems and the pristine BLP [47]: $\Delta E = W - W_P$, where W is the work function of the hybrid system and W_P is the work function of the pristine BLP. The band bendings ΔE are obtained to be -1.838 eV and -2.076 eV for BLP/Zr_2CF_2 hcp-II and BLP/Hf_2CF_2 hcp-II, respectively.

Because of big band bending, the CBM of the BLP moves near the Fermi level upon the formation of the heterobilayers. Moreover, there appears a short partial flat band along the Γ point to the M point near the Fermi level, which is totally contributed from the BLP sheet, as shown in Fig. 3(b) and (d). To gain a clear insight of the flat band near the Fermi surface, the 2D band structures in the IBZ are depicted in Fig. 5(a) and (b) for the BLP/Zr_2CF_2 hcp-II and BLP/Hf_2CF_2 hcp-II, respectively. There also exist a short flat band (black solid line) in the several meV vicinity of the Fermi surface.

Our calculations also suggest that it provides an effective method to grow the BLP monolayer on the Mxene surface epitaxially. To date, direct growth of BLP monolayer remains a big challenge. Although single layer BLP has been realized on the Au(1 1 1) surface, the single layer BLP coexists with the triangularly shaped P-clusters during the growth at high temperature [12]. In addition, a half-layer-by-half-layer growth mechanism are provided to grow single layer BLP on GaN(0 0 1), but the structure of the single layer BLP may be destroyed by the strong P-substrate bonding [48]. If the Mxene are used for the substrate to grow single layer BLP epitaxially, good lattice match makes it easier to be synthesized in experiment comparing with the other substrate. In the mean time, the substrate Mxene has little effect on the electronic properties of the single layer BLP.

5. Conclusion

In summary, we propose two kinds of stable heterojunctions in which the constituent monolayers are BLP and Mxene. The similar lattice constants and sharing the hexagonal lattice for both systems make it possible to form the heterojunctions with little strain. Six different high-symmetry vertically stacked patterns for each configuration are constructed. The energetically stable heterobilayers are obtained to be BLP/Y_2CO_2 atop-II and BLP/Y_2CF_2 hcp-II. The interlayer interaction between the interfaces are weak vdW interaction; thus, the energy bands change little compared with the isolated compounds. Further analysis reveals: (i) the electronic states of the thicker substrate Mxene preserve very well while the energy bands from BLP are shifted down a lot due to the big difference of work functions for BLP and Mxene, thus, the indirect band-gaps decrease compared with the pristine layers; (ii) for the semiconducting heterobilayers, the VBM are contributed form the Mxene while the CBM arise from the BLP, which results in the type-II band alignments; (iii) for the metal heterobilayers, the strong band bending and the lattice stretch for the BLP lead to the downshift of the CBM of the BLP and the bands to cross the Fermi level, which also leads to the partial flat band. Our analysis also suggests that Mxene is a promising substrate to grow BLP monolayer epitaxially.

Data availability

The raw/processed data required to reproduce these findings cannot be shared at this time as the data also forms part of an ongoing study. Details of some results in this paper are shown in the supplementary materials.

Acknowledgments

This research was supported by the National Natural Science Foundation of China under Grant No. 11774195, No. 11374175, and the National Key Research and Development Program of China under Grant No. 2016YFB0700102.

Appendix A. Supplementary material

Supplementary data associated with this article can be found, in the online version, at http://dx.doi.org/10.1016/j.commatsci.2018.05.040.

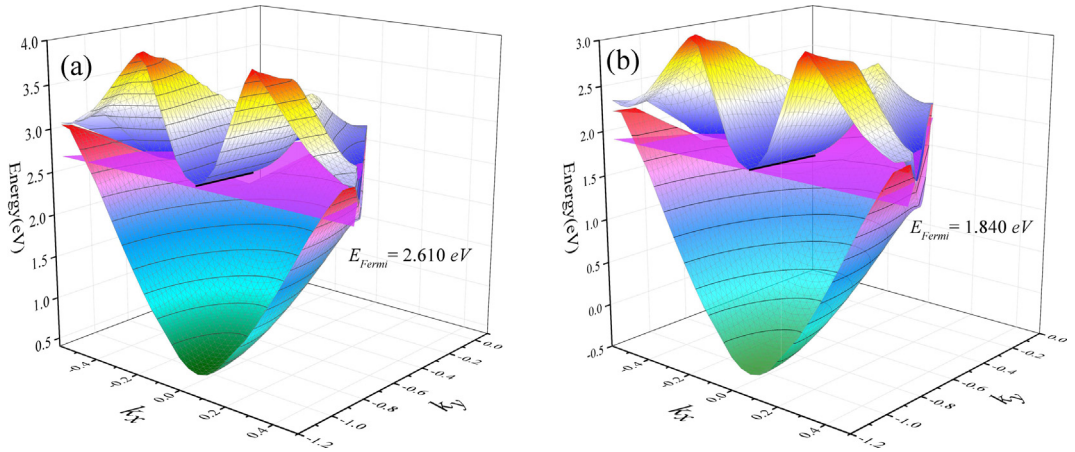

Fig. 5. 2D band structures in the irreducible BZ and distribution of the FS electrons for (a) Zr_2CF_2 hcp-II and (b) Hf_2CF_2 hcp-II, respectively. The pink surface represents the Fermi Surface and the black solid lines are denoted for the flat band crossing the CBM and FS. (For interpretation of the references to color in this figure legend, the reader is referred to the web version of this article.)

References

[1] K.S. Novoselov, A.K. Geim, S.V. Morozov, D. Jiang, Y. Zhang, S.V. Dubonos, I.V. Grigorieva, A.A. Firsov, Science 306 (2004) 666.
[2] P. De Padova, C. Quaresima, P. Perfetti, B. Olivieri, C. Leandri, B. Aufray, S. Vizzini, G. Le Lay, Nano Lett. 8 (2008) 271.
[3] P. Vogt, P. De Padova, C. Quaresima, J. Avila, E. Frantzeskakis, M.C. Asensio, A. Resta, B. Ealet, G. Le Lay, Phys. Rev. Lett. 108 (2012) 155501.
[4] K. Novoselov, D. Jiang, F. Schedin, T. Booth, V. Khotkevich, S. Morozov, A. Geim, Proc. Natl. Acad. Sci. U.S.A. 102 (2005) 10451.
[5] C. Jin, F. Lin, K. Suenaga, S. Iijima, Phys. Rev. Lett. 102 (2009) 195505.
[6] K.F. Mak, C. Lee, J. Hone, J. Shan, T.F. Heinz, Phys. Rev. Lett. 105 (2010) 136805.
[7] Q.H. Wang, K. Kalantar-Zadeh, A. Kis, J.N. Coleman, M.S. Strano, Nat. Nanotechnol. 7 (2012) 699.
[8] M. Chhowalla, H.S. Shin, G. Eda, L.-J. Li, K.P. Loh, H. Zhang, Nat. Chem. 5 (2013) 263.
[9] M. Naguib, V.N. Mochalin, M.W. Barsoum, Y. Gogotsi, Adv. Mater. 26 (2014) 992.
[10] B. Anasori, M.R. Lukatskaya, Y. Gogotsi, Nat. Rev. Mater. 2 (2017) 16098.
[11] L. Li, Y. Yu, G.J. Ye, Q. Ge, X. Ou, H. Wu, D. Feng, X.H. Chen, Y. Zhang, Nat. Nanotechnol. 9 (2014) 372.
[12] J.L. Zhang, S. Zhao, C. Han, Z. Wang, S. Zhong, S. Sun, R. Guo, X. Zhou, C.D. Gu, K.D. Yuan, et al., Nano Lett. 16 (2016) 4903.
[13] A.J. Mannix, X.-F. Zhou, B. Kiraly, J.D. Wood, D. Alducin, B.D. Myers, X. Liu, B.L. Fisher, U. Santiago, J.R. Guest, et al., Science 350 (2015) 1513.
[14] B. Feng, J. Zhang, Q. Zhong, W. Li, S. Li, H. Li, P. Cheng, S. Meng, L. Chen, K. Wu, Nat. Chem. (2016).
[15] A.K. Geim, I.V. Grigorieva, Nature 499 (2013) 419.
[16] K.T. Chan, J. Neaton, M.L. Cohen, Phys. Rev. B 77 (2008) 235430.
[17] M. Ghidiu, M.R. Lukatskaya, M.-Q. Zhao, Y. Gogotsi, M.W. Barsoum, Nature 516 (2014) 78.
[18] K.S. Novoselov, V. Fal, L. Colombo, P. Gellert, M. Schwab, K. Kim, et al., Nature 490 (2012) 192.
[19] J. Zhao, H. Liu, Z. Yu, R. Quhe, S. Zhou, Y. Wang, C.C. Liu, H. Zhong, N. Han, J. Lu, et al., Progr. Mater. Sci. 83 (2016) 24.
[20] H.O. Churchill, P. Jarillo-Herrero, Nat. Nanotechnol. 9 (2014) 330.
[21] Z. Zhu, D. Tománek, Phys. Rev. Lett. 112 (2014) 176802.
[22] Z. Guo, N. Miao, J. Zhou, B. Sa, Z. Sun, J. Mater. Chem. C 5 (2017) 978.
[23] H. Wang, C. Si, J. Zhou, Z. Sun, J. Phys. Chem. C 121 (2017) 25164.
[24] J. Padilha, A. Fazzio, A.J. da Silva, Phys. Rev. Lett. 114 (2015) 066803.
[25] T. Roy, M. Tosun, J.S. Kang, A.B. Sachid, S.B. Desai, M. Hettick, C.C. Hu, A. Javey, ACS Nano 8 (2014) 6259.
[26] E. Wang, X. Lu, S. Ding, W. Yao, M. Yan, G. Wan, K. Deng, S. Wang, G. Chen, L. Ma, et al., Nat. Phys. 12 (2016) 1111.
[27] W. Kohn, L.J. Sham, Phys. Rev. 140 (1965) A1133.
[28] J.P. Perdew, K. Burke, M. Ernzerhof, Phys. Rev. Lett. 77 (1996) 3865.
[29] P.E. Blöchl, O. Jepsen, O.K. Andersen, Phys. Rev. B 49 (1994) 16223.
[30] G. Kresse, D. Joubert, Phys. Rev. B 59 (1999) 1758.
[31] G. Kresse, J. Furthmüller, Phys. Rev. B 54 (1996) 11169.
[32] G. Kresse, J. Furthmüller, Comput. Mater. Sci. 6 (1996) 15.
[33] S. Grimme, J. Comput. Chem. 27 (2006) 1787.
[34] J. Heyd, G.E. Scuseria, M. Ernzerhof, J. Chem. Phys. 118 (2003) 8207.
[35] G. Henkelman, A. Arnaldsson, H. Jónsson, Comput. Mater. Sci. 36 (2006) 354.
[36] H.J. Monkhorst, J.D. Pack, Phys. Rev. B 13 (1976) 5188.
[37] S. Baroni, S. De Gironcoli, A. Dal Corso, P. Giannozzi, Rev. Modern Phys. 73 (2001) 515.
[38] A. Togo, F. Oba, I. Tanaka, Phys. Rev. B 78 (2008) 134106.
[39] Supplementary information for Lattice-matched heterojunctions between blue phosphorene and MXene Y_2CX_2 (X = F, O, and Y = Zr, Hf').
[40] J. Liu, J. Phys. Chem. C 119 (2015) 28417.
[41] N. Gao, J. Li, Q. Jiang, Phys. Chem. Chem. Phys. 16 (2014) 11673.
[42] X.F. Chen, Y.F. Zhu, Q. Jiang, RSC Adv. 4 (2014) 4146.
[43] E. Torun, H. Sahin, F. Peeters, Phys. Rev. B 93 (2016) 075111.
[44] M. Yagmurcukardes, E. Torun, R.T. Senger, F.M. Peeters, H. Sahin, Phys. Rev. B 94 (2016) 195403.
[45] J.E. Padilha, R.H. Miwa, A.J. da Silva, A. Fazzio, Phys. Rev. B 95 (2017) 195143.
[46] C. Bacaksiz, A. Dominguez, A. Rubio, R. Senger, H. Sahin, Phys. Rev. B 95 (2017) 075423.
[47] J. Padilha, A. Fazzio, A.J. da Silva, Phys. Rev. Lett. 114 (2015) 066803.
[48] J. Zeng, P. Cui, Z. Zhang, Phys. Rev. Lett. 118 (2017) 046101.